Effect of heat treatment process on mechanical properties and microstructure of $FeAlCoCrNiTi_{0.5}$ alloy

Maohua Xiao, Jingwen Chen, Jingjing Kang, Ke Chen, Dan Wu, and Nong Gao

Citation: AIP Advances **8**, 095322 (2018); doi: 10.1063/1.5050434
View online: https://doi.org/10.1063/1.5050434
View Table of Contents: http://aip.scitation.org/toc/adv/8/9
Published by the American Institute of Physics

Effect of heat treatment process on mechanical properties and microstructure of $FeAlCoCrNiTi_{0.5}$ alloy

Maohua Xiao,[1,2,a] Jingwen Chen,[1] Jingjing Kang,[1] Ke Chen,[1] Dan Wu,[1] and Nong Gao[2]
[1]*College of Engineering, Nanjing Agricultural University, 210031 Nanjing, China*
[2]*Faculty of Engineering and the Environment, University of Southampton, SO17 1BJ Southampton, UK*

(Received 31 July 2018; accepted 14 September 2018; published online 25 September 2018)

In order to study the effects of different sintering processes on the properties of the alloy, including the microstructure, hardness, friction and wear properties of the alloy, the optimum sintering method and process parameters were selected. A series of FeAlCoCrNiTi0.5 high-entropy alloy blocks were prepared by mechanical alloying using inert alloy sintering technology. XRD pattern showed that when the sintering temperature was 1000°C and the holding time was 3h, the phase structure would be a simple body-centered cubic BCC2 phase and a face-centered cubic FCC phase. SEM observation showed that the microstructure is denser, and the grain refinement of the high entropy alloy is remarkably better. The evaluation of hardness, friction and wear properties showed that the high-entropy alloy had the best overall performance. https://doi.org/10.1063/1.5050434

I. INTRODUCTION

The high-entropy alloy (HEA) have broad prospects for industrial applications due to their properties such as high strength and toughness,[1] high hardness,[2,3] wear resistance,[4] and excellent resistance to temper softening.[5] At present, some HEAs with excellent performance have been applied in production and life,[6] such as high-entropy alloy drill bits, high-entropy alloy micro-electromechanical elements, etc. Therefore, it is of great significance for both the theoretical research of HEAs and the development and utilization of new alloys. However, high-entropy alloys have not yet been extended from the laboratory to the market, that's why a large number of researchers are working in this direction, hoping to promote potential applications in ultra-light materials such as aerospace materials. There are a lot of obstacles on the road to HEAs research. The main concern at present is to how to improve the structural properties and the extensiveness of their applications, and then their preparation process has a very important influence on their structural performance. Vacuum arc furnace fusion casting[7–11] is the most effective and common practice today, but traditional melting methods may limit the size and shape of the sample and its further application. It was found that the use of mechanical alloying and a reasonable sintering process can produce HEAs are of larger size, finer grain size, and better strength and hardness performance compared with the electric arc. With the deepening of research on high-entropy alloys, high-entropy alloys such as AlFeTiCrZnCu,[12,13] $AlxCoCrCu_{0.5}FeNi$,[14] AlFeNiCoCr,[15] AlCoFeNiCu,[16] etc. were sequentially prepared by mechanical alloying methods. Alloying plays an important role in improving the properties and applications of high-entropy alloys.[14] It can avoid segregation of component elements. It is easier to obtain amorphous or nanocrystalline structures than traditional methods, so it is It is widely used for the preparation of composite powders and the like.[17,18] On the other hand, since the product prepared by mechanical alloying is a powder sample, it is necessary to select an appropriate method

[a]Corresponding author's email address: xiaomaohua@njau.edu.cn

to make it into a bulk sample, which involves the following processing technology. Selecting a suitable post-treatment process has a great influence on the properties of HEAs. In recent years, many scholars have used vacuum hot pressing, plasma sintering and other methods to obtain high entropy alloys such as NiCrCoTiV, CoCrFeNiTi_x, AlCoCrFeNi, etc.[19–21] However, scholars have adopted the traditional vacuum sintering process. There is relatively little research done on block high entropy alloys. Moreover, the vacuum sintering equipment is low in cost, easy to operate and also has a broad research prospect in the preparation of high-density block high entropy alloys. Therefore, in this study, the method of vacuum sintering was adopted for the post-treatment of high-entropy alloy preparation.

AlFeNiCoCr series high entropy alloys[15] have been widely studied. Recently reported AlCoCrFeNiTi0.5 high entropy alloys have outstanding comprehensive mechanical properties in the explored high-entropy alloy systems and can be on a par with most of the high-strength alloys even bulk amorphous alloys are comparable that have been publicly reported.[22] The AlCoCrFeNiTi0.5 high-entropy alloy has no obvious segregation coefficient, which can effectively avoid the segregation of Cu in AlCoCrFeNiCu alloy. The dendrite structure of the alloy is all bcc phase. AlFeNiCoCr series HEAs[23] have been widely studied. Moreover, the high entropy alloy has no casting limit and has a wide application prospect. Although a lot of researches have been done on high-entropy alloys, the research on high-entropy alloys prepared by mechanical alloying and the research on heat treatment processes on the high-entropy alloys are relatively rare. Therefore, this study used mechanical alloying combined with vacuum sintering technology to prepare $FeAlCoCrNiTi_{0.5}$ high entropy alloy, change its sintering process, study the mechanical properties and microstructure of the alloy. At the same time, the influences of different sintering processes on the microstructure, hardness, friction and wear properties and the mechanism of action of the alloys are explored in order to provide the necessary data accumulation and technical support for the engineering application of these alloys.

II. MATERIALS AND METHODS

Metal powder was purchased from Aladdin website. High entropy alloy powders were processed by mechanical alloying. An electronic molecular balance (ME204E type) with an accuracy of 0.01 g was used to weigh and make Fe, Al, Co, Cr, Ni, Ti element mixed at a molar ratio of 1:1:1:1:1:0.5. Table I shows the composition of the powder material in the alloy. The weighed mixed powder was placed in a variable frequency planetary ball mill (XQM-0.4L type) for alloying. Vacuum stainless steel tanks and stainless steel balls were used for the ball milling. The ball-to-bulb ratio was 10:1. The ball milling time was set to 20 h and the rotation speed was 350 r/min. Prior to ball milling, the vacuum stainless steel tank was first evacuated, and the vacuum stainless steel tank was filled with high-purity argon (≧ 99.0%, 0.5 MPa) to provide a protective atmosphere for ball milling.

After the metal powder was alloyed, 5 g of the alloy powder was weighed, 0.2 g of stearic acid was added as a binder and a release agent, and the mixture was ground uniformly in a mortar. The powder was compressed into a tablet using a tablet press (DY-30 type). The pressure was set at 35 kPa and the pressure was maintained for 30 minutes to obtain a bulk sample (Figure 1). After the sample was taken out, it was placed in a vacuum drying oven and incubated at 200 degrees for 2 hours to remove stearic acid. It was then sintered in an inert gas atmosphere in a tube furnace. During the sintering

TABLE I. Composition of alloy powder materials.

Element	Molar mass	Ture/g	Metal purity
Fe	55.85	8.09	99. 99%
Al	26.98	3.90	99.95%
Co	58.93	8.52	99. 50%
Cr	51.99	7.51	99. 50%
Ni	58.69	8.52	99. 50%
Ti	47.87	3.46	99. 99%

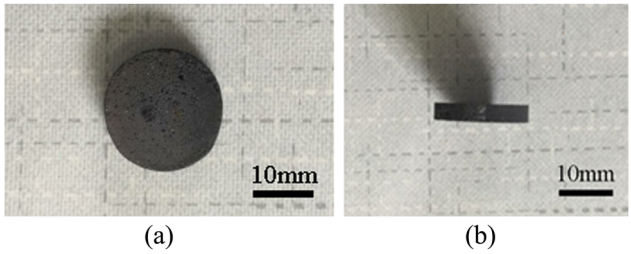

FIG. 1. Specimen.

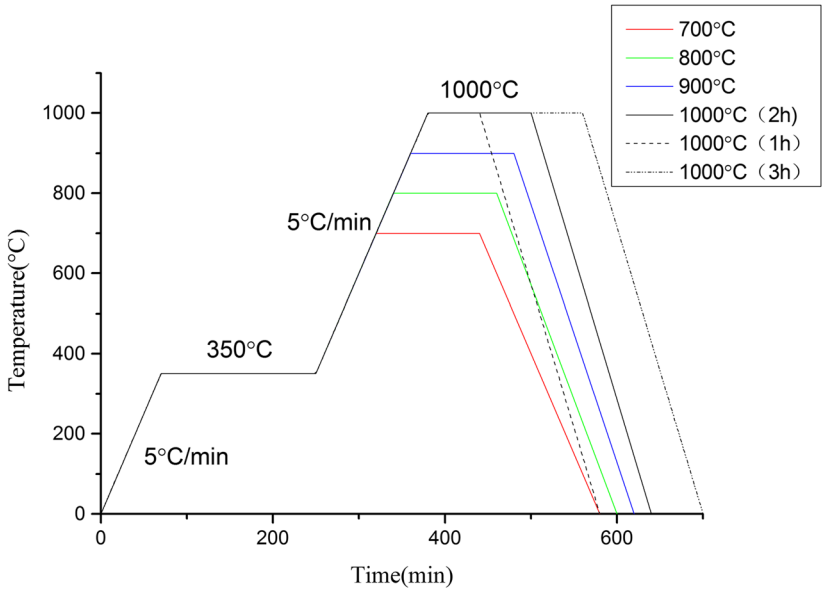

FIG. 2. Sintered process route.

process, the samples were divided into 7 groups of 2 in each group. The sintering temperature was changed in the first four groups, and in the last three groups the holding time was changed. The sintering process route is shown in Figure 1 below. The sintering process is shown in Figure 2.

After sintering, the samples were tested. XRD was used to observe the phase structure of the HEA. Then, the microhardness tester was used to measure the surface hardness of the specimen. Each specimen was measured at a distance of 3 mm from the center of the specimen and measured at 5 points. The distance between each indentation was 2 mm and the loading load was 0.98 N. The time was 10s. After the measurement was completed, the average was taken as the hardness value of the sample. Then the material's surface performance tester was used to test the friction and wear properties of the sample. Finally, the microstructure of the high-entropy alloy was examined by SEM.

III. RESULTS AND DISCUSSION

A. Phase analysis

XRD was used for the phase analysis of sintered high-entropy alloy bulk samples, and the microstructure of high entropy alloys at different sintering temperatures and different holding times was compared. The current and voltage values used in the experiment were well adjusted. The voltage was 40 KV and the current was 40 mA. The incident X-ray was a Cu target Kα ray.

Figure 3 shows X-ray diffraction patterns of AlCoCrFeNiTi0.5 alloys at different sintering temperatures. According to the diffraction data given by the X-ray diffractometer, $\frac{1}{N_C}$ is multiplied by the

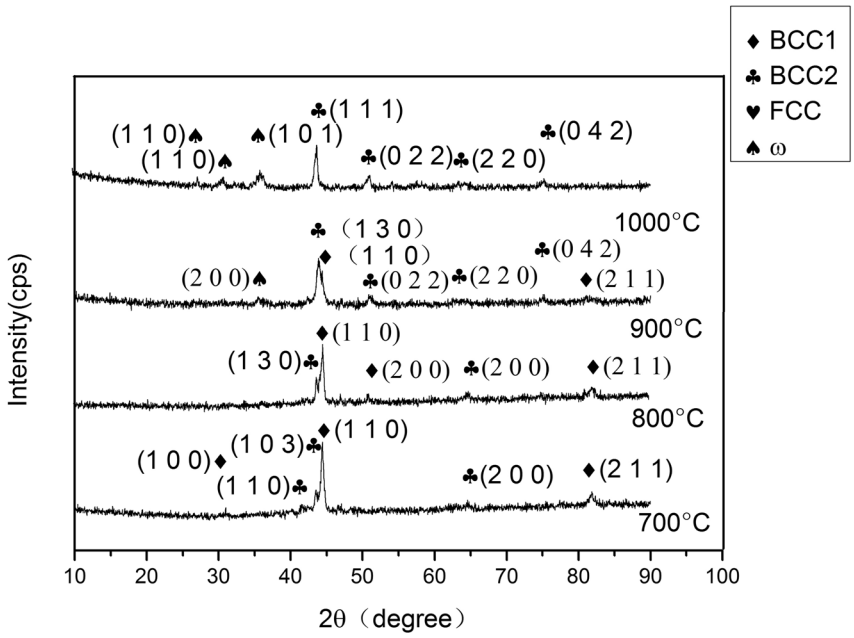

FIG. 3. XRD Image of $AlCoCrFeNiTi_{0.5}$ at Different Sintering Temperatures.

Q_{hkl} measured in the experiment, which is $\frac{1}{d_{hkl}^2}$, and the resulting product is a constant to determine the major phases are two simple cubic structures. The Gibbs free energy formula $\Delta G=\Delta H-T\Delta S$[22] shows that the higher the hybrid entropy is, the lower the free energy is. High mixing entropy can improve the stability of solid solution in alloy system. Moreover, since high entropy alloys have high mixing entropy due to the addition of many different elements, they can suppress the formation of intermetallic compounds, so only two simple body-centered cubic solid solution structures are formed. Combined with the extinction law, we can see that AlCoCrFeNiTi0.5 high entropy alloy is composed of two body-centered cubic structure phases BCC1 and BCC2. Figure 5(a) is a schematic diagram of a lattice image of a BCC phase. This has also been verified in the literature of the predecessors.[24,25] The eight atoms in the unit cell are located at the corners of the cube. According to the correspondence of diffraction peaks, it can be found that BCC1 was correspondingly enriched in Al-Ni phase, while BCC2 was correspondingly enriched in Fe-Cr phase to determine the cubic system to which the sample belonged. The reason for forming a body-centered cubic structure is that the atomic radii of Al and Ti are large relative to other elements, and the difference in atomic size is large, so the degree of lattice distortion is large. And the body-centered cubic structure is loose, and it is easier to adjust the strain on the lattice to reduce the free energy of the system, so the high-entropy alloy tends to form the body-centered cubic phase. In the body-centered cubic structure, one atom is in the center of the cube and eight atoms are close to the center atom. Finally, the high-intensity diffraction line combined with the Bragg equation law could be reflected by the diffraction pattern. Table II shows the lattice parameters of the main phase in the alloy.

Moreover, it can be seen that the height ratio of the diffraction peaks in the figure with the sintering temperature of 700° C is much greater than that of the BCC2 phase. When the maximum

TABLE II. The cell parameters of high entropy alloys at different sintering temperatures.

Sintering temperature (°C)	BCC1/nm	BCC2/nm	ω-phase/nm
700	0.2884	0.6576	-
800	0.2878	0.6529	-
900	0.2864	0.6503	0.2463/0.4024
1000	-	0.6515	0.2344/0.3828

temperature rises to 800°C, there is no significant change in the structural phase of the alloy, which is still composed of BCC1 and BCC. However, by comparing the peak ratio between the highest peak and the second peak at a sintering temperature of 700 °C, it is found that the content of BCC2 in the alloy gradually increased. This is because as the temperature increases, the atomic distribution inside the alloy is more uneven, the lattice distortion strain energy increases, but the structure of BCC2 is looser. This can be seen from the data in Table II. Therefore, the main phase in the alloy is converted from body-centered cubic BCC1 to body-centered cubic BCC2, it can adjust the lattice strain and reduce the free energy of the alloy.[26] When the sintering temperature reaches 900 °C, not only the BCC1 and BCC2 two body-centered cubic phases are detected within the detection range of XRD, but also the presence of ω-phase is detected. Compared with the X-diffraction PDF standard card, the diffraction peaks of ω-phase and $AlTi_3$ are found. Figure 5(b) is a schematic diagram of a lattice image of a ω-phase. Simultaneously, the highest peak corresponds to the BCC2 phase, indicating that the content of BCC1 is gradually decreasing and the content of BCC2 is increasing. When the sintering temperature rises again to 1000 °C, the existence of BCC1 phase has not been detected within the detection accuracy range of XRD. It can be seen that the high-entropy alloy $AlCoCrFeNiTi_{0.5}$ gradually transforms from BCC1 phase to BCC2 phase with increasing sintering temperature. The BCC1 phase disappears completely at 1000 °C, and body-centered cubic BCC2 phase and Intermetallic compound AlNi3 exist. In order to quantitatively compare the conversion of the main phase in the high entropy alloy, the total contribution of the phase is determined as the sum of the volume fraction of the main phase BCC1 and BCC2, regardless of the existence of other phases, only the total integrated intensity of all observed diffraction peaks of the main phase is considered.[27] Table III shows the volume fraction calculated for each phase for the different Sintering temperature, consistent with our previous analysis.

As can be seen from the above four figures, the highest peak occurs near 44° and shifts to the left as the sintering temperature increases. It can be seen from Table I that when the temperature is just rising, the crystal grains are gradually refined, and the lattice parameters are slightly Decrease, but when the temperature rises to a certain extent, the crystal grains will grow and coarsen, and the lattice parameters will increase. However, the diffraction angles at diffraction angles are very low at large angles. This is because the high-entropy alloys contain many kinds of metal atoms. Through the joint action of solid solution and substitution, the number of crystal structures interfering with each other is reduced, which weakens the intensity of the diffraction peak.[24]

Figure 4 shows the X-ray diffraction pattern of $AlCoCrFeNiTi_{0.5}$ alloy at different holding time when the sintering temperature is 1000 °C. Table IV shows the lattice parameters of the major phases in the alloy at different holding times. Figure 4(a) shows the X-ray diffraction pattern at 1000 °C for 1 hour. It is evident that BCC2 is the main phase in the alloy and contains a small amount of BCC1 and ω phases. However, after the incubation time was extended to 2 h, the diffraction peaks of the BCC1 phase could not be detected, and only the corresponding peaks of the BCC2 and ω phases were detected, indicating that prolonging the holding time is beneficial to ensure the complete transition of the BCC1 phase to the BCC2 phase. In combination with Table III, it can be found that the BCC1 lattice parameter is significantly increased at 1 h of incubation, and the lattice parameter close to the BCC2 phase can confirm the conclusion that BCC1 phase changes to BCC2 phase.

When the holding time is 3h, the peak of the X-ray diffraction pattern of AlCoCrFeNiTi0.5 high entropy alloy coincides with the diffraction peak of Fe. Fe will transform into a cubic structure at 912°C~1394°C, which is called γ-Fe. The results prove that the extended holding time is conducive to the transition. Therefore, the structural phase of the high-entropy alloy changes from the body-centered cubic BCC2 structure to the face-centered cubic FCC. Figure 5(c) is a schematic diagram of a lattice image of a FCC phase.

TABLE III. Percentage of volume fraction of the main phase for the different sintering temperature.

V.fraction	700(2h)	800(2h)	900(2h)	1000(2h)
V_{bcc1}[%]	65.20	60.34	44.05	0
V_{bcc2}[%]	34.80	39.66	55.95	100

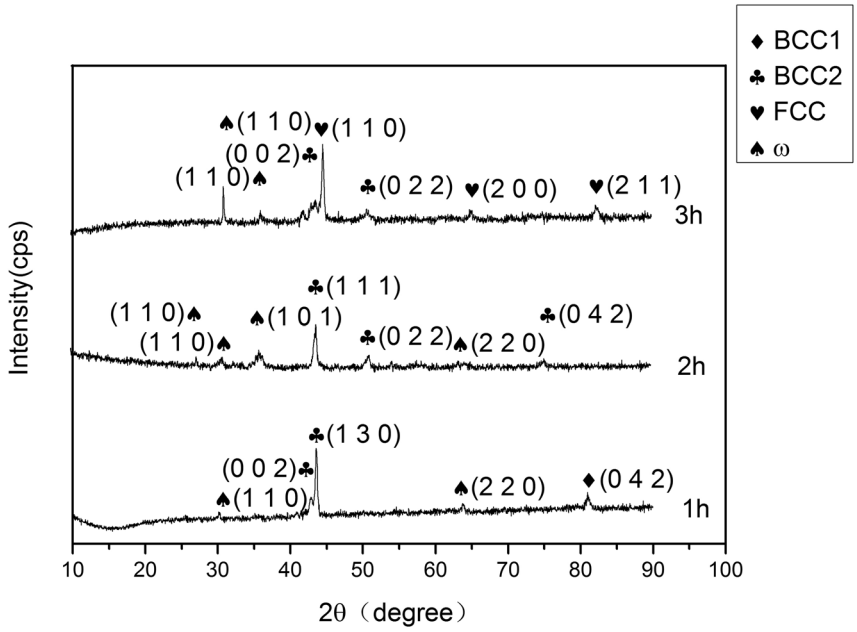

FIG. 4. XRD Image of $AlCoCrFeNiTi_{0.5}$ alloy at Different Holding Time.

TABLE IV. The Cell Parameters of High Entropy Alloys at Different Holding Time.

Holding time(h)	BCC1/nm	BCC2/nm	ω-phase/nm	FCC/nm
1h	0.5297	0.6567	0.2793/0.4562	-
2h	-	0.6515	0.2344/0.3828	-
3h	-	0.5068	0.2719/0.4521	0.2862

B. Micromorphology analysis

In this study, the fracture morphology of high-entropy alloys with different compositions was observed by SEM to analyze the micro-morphology of high-entropy alloys. It can be seen from the Figure 6 that the macroscopic microstructure of this alloy is equiaxed.

It can be seen from the 1000x magnification that the microstructure of the alloy is denser, but there are a few pores. However, as the sintering temperature gradually increases, the porosity gradually decreases and the alloy density increases. Comparing the four figures, it can be found that when the sintering time is 700 °C and 800°C, the block structure is less, the particles are obvious, and there are many through holes. At 1000 °C, many large structures are formed in the alloy

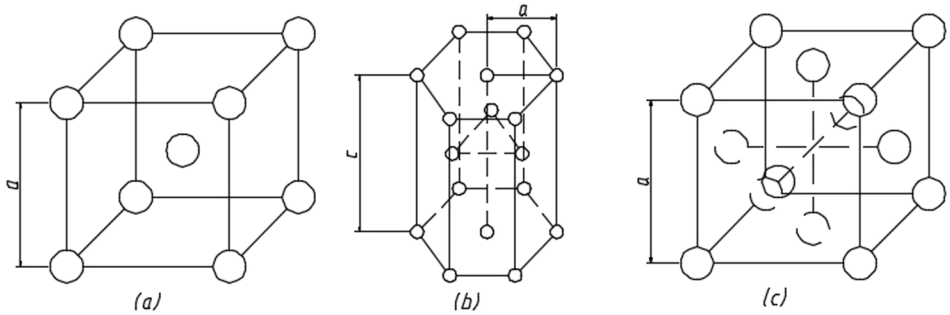

FIG. 5. Schematic diagrams of the lattice images of the BCC phase, ω-phase and FCC phase.

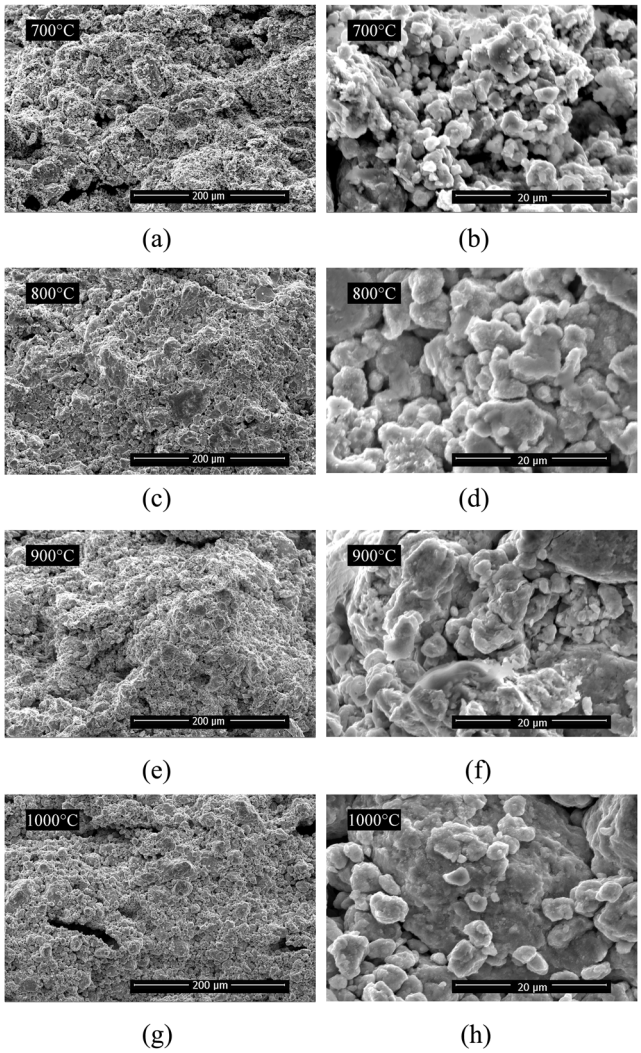

FIG. 6. SEM photographs of different sintering temperature samples with holding time of 2h.

with less porosity. This shows that as the sintering temperature increases, the grains will gradually refine to form a more stable phase. Combined with the above XRD analysis, when the annealing temperature is 700-900 °C, the alloy consists of BCC1 phase and BCC2 phase. When the annealing temperature is 1000 °C, the alloy consists of a simple BCC2 phase. The high temperature annealing promotes the element diffusion rate, homogenizes the alloying elements, and also eliminates some of the dendrite segregation of the alloy. At the same time, we can also see that when the sintering temperature is 700 °C, the grains are refined. However, it can also be observed that as the heat treatment temperature is further increased, the grain size of the alloy is continuously increasing, but the degree of its growth is further small. This is because the grain growth rate of the alloy at this time is related to the diffusion between its atoms. When the temperature is higher, the diffusion coefficient of the atom is larger and the grain boundary is more likely to migrate, so that the grain is coarsened.

For high-entropy alloys, the heat treatment generally does not cause phase transformation of the alloy.[28] It can be seen from the three figures above on, the macroscopic structure of the alloy is still equiaxed at different holding times. However, as the holding time increases, the grains in the alloy are significantly coarsened; the porosity is significantly reduced; and the density is increased.

Observing the 10,000-magnification chart (Figure 7), we can also see that the morphology of the alloy shows a tendency to spheroidize with the increase of holding time. Moreover, when the holding

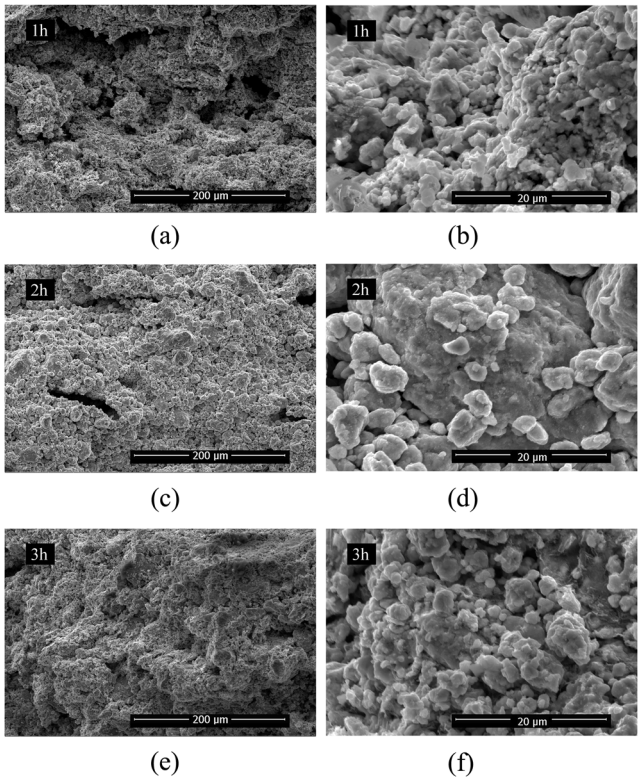

FIG. 7. SEM picture of different holding time samples with sintering temperature of 1000 °C.

time reaches 3 h, the existence of a network structure can be observed in the alloy. Combined with XRD analysis, it can be known that the alloy contains more ordered BCC1 phase when it is incubated for 1 hour; and as the holding time is extended to 2 hours, disordered BCC2 becomes the main phase, with the content of BCC1 phase decreasing, and a large number of nanophases appearing in the alloy. When the holding time was 3 h, a nano-phase interweaved network structure appeared in the alloy, and a more stable phase was formed in the alloy.

C. Hardness analysis

The stress field generated by the lattice distortion interacts with the elastic stress field around the dislocations, which causes pinning effects on the displacement slip, and thus the resistance to dislocation slip increases. The addition of Ti element has strengthened the lattice distortion and enhanced the effect of solid solution strengthening, making the high entropy alloy higher in hardness. Compared with the casting method, the high-entropy alloy can obtain finer grains through mechanical alloying. The ball milling process causes a strong lattice distortion and forms a supersaturated solid solution. In the sintering process, phase transitions often occur to produce nano-precipitates, which all make the strengthening effect more obvious. The results are shown in Table V and Table VI.

As can be seen from Table V, with the increase of soak temperature, the hardness is gradually increasing, reaching 518.67HV at 1000 °C. Compared with a sample of 700 °C, a 192.87% increase in hardness is found. This is because the phase structure of high-entropy alloys continuously shifts

TABLE V. Microhardness values of specimens incubated for 2 hours at different sintering temperatures.

Sintering temperature (°C)	700	800	900	1000
Microhardness (HV)	177.10	305.75	439.05	518.87

TABLE VI. Sintering temperature of 1000 °C different holding time microhardness of the sample.

Holding time (h)	1	2	3
Microhardness (HV)	544.65	644.78	682.99

from BCC1 phase to BCC2 phase with the sintering temperature increasing. After X-ray diffraction analysis, it can be confirmed that BCC1 is correspondingly enriched in Al-Ni phase, while BCC2 is correspondingly enriched in Fe-Cr phase, which has higher hardness and stability compared with Fe-Cr solid solution,[22] so the hardness of high-entropy alloys is constantly increasing. After the sintering temperature reached 900 °C, the presence of the intermetallic compound $AlNi_3$ was detected in the high-entropy alloy $AlCoCrFeNiTi_{0.5}$. The covalent bond in the $AlNi_3$ phase can ensure that the alloy has a higher hardness, and thus the hardness of the high-entropy alloy after the temperature is raised, which means it has been further improved.

Table VI shows the microhardness of the samples sintered at 1000 °C for 1 h, 2 h, and 3 h. It can be found that the hardness of the sample incubated for 3 hours increases by 25.40% relative to the holding time of 2 hours, and the overall hardness increases with the holding time. Obviously, as the holding time increases, the atoms diffuse more completely, filling up the pores, giving the alloy a denser structure, increasing the density of the high-entropy alloy, and the hardness as well. When the holding time is extended to two hours, there is a clear upward trend in hardness. After three hours of holding time, the hardness does not increase significantly. This is because the phase in the high-entropy alloy $AlCoCrFeNiTi_{0.5}$ has changed after three hours of heat preservation, and the phase shifts from the BCC to FCC phase. It is generally believed that the type of high entropy alloy phase structure is one of the main factors affecting the hardness of the alloy. The high entropy alloy of the BCC structure has high in strength but brittle, and the high entropy alloy of the FCC structure has low strength but good plasticity, so the high entropy alloy after transformation is high. Hardness increase is not obvious.

D. Friction and wear analysis

Wear is an important cause of failure of metal parts, so the friction coefficient of metal materials is an important parameter used to represent the friction properties of materials. The friction and wear process of materials is a complex mechanical chemical coupling process not only affected by the material structure but also related to the process parameters associated with the wear environment.[29] The smaller amount of wear, resulted in by a smaller the friction coefficient, indicates the better the friction properties of the material. Therefore, we studied the friction and wear properties of vacuum-sintered high-entropy alloys and investigated the effects of different sintering processes on the wear resistance of high-entropy alloy $FeAlCoCrNiTi_{0.5}$. In the experiment, the friction coefficient of the high-entropy alloy was measured by using a material surface performance tester (CFT-1 type). The movement mode was reciprocating. The experimental load was 170 N, the rotation speed was 500t/min, and the experiment time was 20 minutes. The frictional counterpart was a 4mm diameter steel ball with a hardness of 62HRC. The measured frictional wear coefficients are shown in Figures 8 and 9, the average friction and wear coefficient is shown in Table VII and Table IX, and the wear amount is shown in Tables VIII and X.

Friction and wear are the relative motion behaviors of the surfaces of two materials, which are directly affected by the state of the contact surface. W = k (P/H), W refers to the wear rate, P represents the load, H represents the hardness of the material, and k is a parameter related to the plasticity of the material. According to the classical Archard equation, the hardness of the material plays an important role in many factors in contact with the surface.[30,31] Our previous research shows that with the increase of sintering temperature, the $FeAlCoCrNiTi_{0.5}$ high-entropy alloy increases hardness due to phase transformation and nano-scale precipitation, which leads to an increase in friction and wear properties. The experimental results of Tables VI and VIII are consistent.

In addition, the wear surface of $FeAlCoCrNiTi_{0.5}$ alloy had obvious adhesion and furrow morphology after the experiment. The wear mechanism of this alloy can be approximated to be furrow

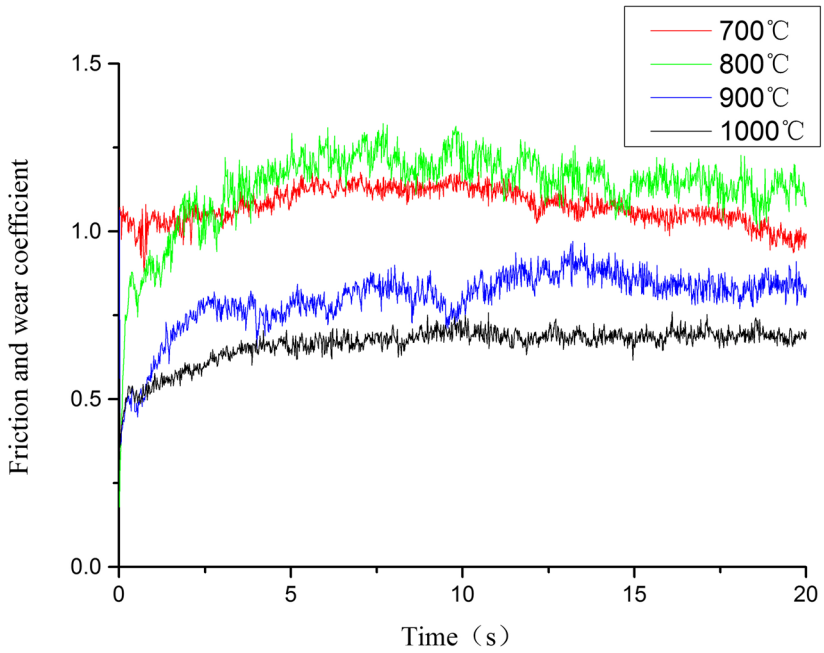

FIG. 8. Friction and Wear Coefficient of $AlCoCrFeNiTi_{0.5}$ at Different Sintering Temperatures.

wear and adhesive wear.[32,33] It can be seen from Figure 8 that the high entropy alloy exhibits excellent friction and wear properties, and the friction coefficient is relatively stable during the friction test process. With the increase of the sintering temperature, the average friction coefficient shows a decreasing trend as a whole. Table VII shows that as the sintering temperature increases, the amount of wear gradually decreases. When the sintering temperature is low, the structure is not dense enough, there are more pores. Therefore, the friction coefficient is higher, and the amount of wear is also larger. With the increase of sintering temperature, some of the intermetallic compounds or other crystalline phases are melted and infiltrated to fill some of the pores in the high-entropy alloy, making

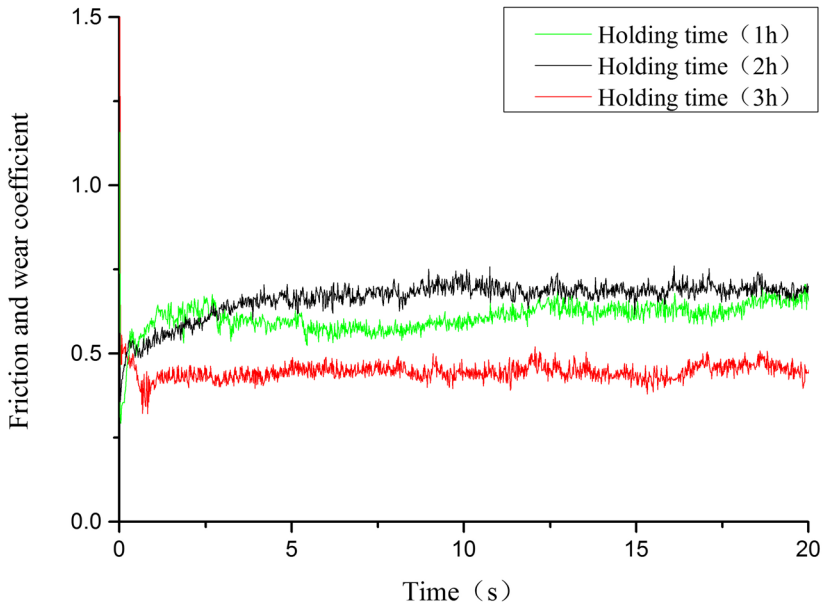

FIG. 9. Friction and Wear Coefficient of $AlCoCrFeNiTi_{0.5}$ at 1000°C with Different Holding Time.

TABLE VII. The Friction and Wear Coefficient of different sintering temperature specimens with 2 h holding time.

Sintering temperature (°C)	700(2h)	800(2h)	900(2h)	1000(2h)
Friction and Wear Coefficient	1.0749	1.1337	0.8001	0.6633

TABLE VIII. The wear of different sintering temperature specimens with 2 h holding time.

Sintering temperature (°C)	700(2h)	800(2h)	900(2h)	1000(2h)
Quality before friction and wear measurement (g)	5.1326	5.1452	5.1458	5.1461
Quality after friction and wear measurement (g)	5.1253	5.1387	5.1405	5.1417
Wear amount (g)	0.0073	0.0065	0.0053	0.0044

TABLE IX. Friction and wear coefficient of samples with different maximum holding time of 1000 °C.

Holding time (h)	1(1000°C)	2(1000°C)	3(1000°C)
Friction and Wear Coefficient	0.607398	0.6633	0.4469

TABLE X. Maximum temperature 1000°C Wear time of specimens with different holding time.

Holding time (h)	1(1000°C)	2(1000°C)	3(1000°C)
Quality before friction and wear measurement (g)	5.1445	5.1461	5.1456
Quality after friction and wear measurement (g)	5.1393	5.1417	5.1420
Wear amount (g)	0.0052	0.0044	0.0036

the structure more compact and the surface smoother. Thus, the friction coefficient decreases, and the amount of wear decreases. Based on comprehensive analysis, the friction and wear properties of $FeAlCoCrNiTi_{0.5}$ high entropy alloy at 1000 °C are the best.

Figure 9, Table IX and Table X respectively show the friction and wear coefficient and wear amount at a sintering temperature of 1000 °C. It can be seen that the longer the holding time is, the lower the average coefficient of friction and wear of the high-entropy alloy is. When the temperature is kept for 1h and 2 h, the friction coefficient do not change significantly. When the holding time is 3 h, the average friction coefficient decreased with the smallest wear, and the friction performance was the best. This is because as the holding time increases, atomic diffusion can better fill the pores and the alloy has a denser structure. Moreover, the friction and wear properties are closely related to the hardness. As the hardness of the material increases, the material is less likely to be worn. The coefficient of friction and wear and the amount of wear for 3 h of heat preservation is the smallest corresponding to the highest value of hardness in Table VI.

IV. CONCLUSION

(1) The XRD experiments show that the main composition phase of $FeAlCoCrNiTi_{0.5}$ is body-centered cubic structure phase BCC1 or BCC2. As the sintering temperature increases, the main phase in the alloy shifts from BCC1 to BCC2 and the presence of the intermetallic compound $AlTi_3$ is found at 900 °C. At 1000 °C, with the increase of holding time, the alloy firstly transforms from BCC1 phase to BCC2 phase, and after 3h, FCC phase appears.

(2) The $FeAlCoCrNiTi_{0.5}$ high-entropy alloy is a porous structure with a few pores. The sintered high-entropy alloy has a dense structure. With the increase of the sintering temperature, the grains are gradually refined and a more stable phase is formed. As the holding time increases, a network structure appears in the high entropy alloy.

(3) In the microhardness and frictional wear tests, both the sintering temperature and the holding time are positively correlated with the properties of the alloy. The higher the sintering temperature and the holding time is, the higher the hardness of this alloy is and the lower the average friction coefficient is.
(4) The increase of sintering temperature and the holding time is conducive to grain refinement and atom diffusion. This can increase the density of the alloy, form a more stable phase and thus enhance various comprehensive properties. In future research, we will continue to deepen the study of the effects of heat treatment on alloy properties, such as corrosion resistance, electrochemical performance, etc., to verify the conclusion of this experiment.

ACKNOWLEDGMENTS

The research is funded partially by the Fundamental Research Funds for the Central Universities fund (KYZ201760), the Open topic of Jiangsu Provincial Key Laboratory of Advanced Manufacturing Technology (HGAMTL-1711) and Program for Student Innovation through Research and Training of Nanjing Agricultural University (1730B28).

The authors declare that there are no competing interests regarding the publication of this paper.

[1] K. Y. Tsai, M. H. Tsai, and J. W. Yeh, "Sluggish diffusion in Co-Cr-Fe-Mn-Ni high-entropy alloys[J]," Acta Materialia **61**(13), 4887–4897 (2013).
[2] C. J. Tong, M. R. Chen, S. K. Chen *et al.*, "Mechanical performance of the Alx Co Cr Cu Fe Ni high-entropy alloy system with multiprincipal elements[J]," Metallurgical and Materials Transactions A **36**(5), 1263–1271 (2005).
[3] L. H. Wen, H. C. Kou, J. S. Li *et al.*, "Effect of aging temperature on microstructure and properties of AlCoCrCuFeNi high-entropy alloy[J]," Intermetallics **17**(4), 266–269 (2009).
[4] M. H. Chuang, M. H. Tsai, W. R. Wang *et al.*, "Microstructure and wear behavior of AlxCo1.5Cr Fe Ni1.5 Tiy high-entropy alloys[J]," ActaMaterialia **59**(16), 6308–6317 (2011).
[5] M. H. Tsai, C. W. Wang, C. W. Tsai *et al.*, "Thermal stability and performance of NbSiTaTiZr high-entropy alloy barrier for coppermetallization[J]," Journal of the Electrochemical Society **158**(11), H1161–H1165 (2011).
[6] Y. Zhang, Y. J. Zhou, and G. L. Chen, "Fast moving prospects of multi-principal component alloys with high mixing entropy[J]," Physics **37**(8), 600–605 (2008).
[7] X. F. Wang, Y. Zhang, Y. Qiao, and G. L. Chen, "Novel microstructure and properties of multicomponent CoCrCuFeNiTix alloys[J]," Intermetallics **15**, 357–362 (2007).
[8] Y.-F. Kao, S.-K. Chen, J.-H. Sheu *et al.*, "Hydrogen storage properties of multi-principal-component CoFeMnTixVyZrz alloys[J]," International Journal of Hydrogen Energy **35**, 9046–9059 (2010).
[9] C. Shin-Tsung, T. Wei-Yeh, Y.-F. Keu *et al.*, "Microstructure and properties of age-hardenable AlxCrFe$_{1.5}$MnNi$_{0.5}$ alloys[J]," Materials Science and Engineering A **527**, 5818–5825 (2010).
[10] J. M. Zhu, H. M. Fu, H. F. Zhang *et al.*, "Microstructures and compressive properties of multicomponent AlCoCrFeNiMox alloys[J]," Materials Science and Engineering A **527**, 6975–6979 (2010).
[11] Y. L. Chou, Y. C. Wang, J. W. Yeh, and H. C. Shih, "Pitting corrosion of the high-entropy alloy Co$_{1.5}$CrFeNi$_{1.5}$Ti$_{0.5}$Mo$_{0.1}$ in chloride-containing sulphate solutions[J]," Corrosion Science **52**, 3481–3491 (2010).
[12] Y. M. Y. Yuan Microstructure and properties of AlxCrCrCu0.5FeNi high-entropy alloy prepared by mechanical alloying [D]. Hunan University, 2016.
[13] S. Varalakshmi, M. Kamaraj, and B. S. Murty, "Synthesis and characterization of nanocrystalline AlFeTiCrZnCu high entropy solid solution by mechanical alloying[J]," Journal of Alloys and Compounds **460**, 253–257 (2008).
[14] S. Varalakshmi, M. Kamaraj, and B. S. Murty, "Processing and properties of nanocrystalline CoNiCoAlZnTi high entropy by mechanical alloying [J]," Materials Science and Engineering A **527**, 1027–1030 (2010).
[15] Z. Chen Microstructure and Properties of AlFeNiCoCr System High Entropy Alloys Prepared by Mechanical Alloying [D]. South China University of Technology, 2016.
[16] S. C. Fang Research on Microstructure and Properties of AlCoFeNiCu High-entropy Alloys Prepared by Mechanical Alloying [D]. South China University of Technology, 2014.
[17] B. G. Huang, J. W. Ye, and D. Z. Sun Study on Thermally Dissolving Layers of Multivariate High Entropy Alloys [D]. National Tsing Hua University, 2003.
[18] T. K. Chen, T. T. Shun, J. W. Ych, and M. S. Wong, "Nanostructured nitride films of multi-element high-entropy alloys by reactive DC sputtering[J]," Suface & Coatings Technology **188-189**, 193–200 (2004).
[19] Z. Cai, G. Jin, X. Cui *et al.*, "Experimental and simulated data about microstructure and phase composition of a NiCrCoTiV high-entropy alloy prepared by vacuum hot-pressing sintering[J]," Vacuum **124**, 5–10 (2016).
[20] Y. Jiang, H. Zu, and Y. Zhang, "Research on CoCrFeNiTi_x high entropy alloys by spark plasma sintering [J]," Journal of Harbin University of Science and Technology **22**(05), 121–125+129 (2017).
[21] P. Zhou, Y. Liu, Y. Yu, and D. Xiao, "Phase evolution and mechanical properties of AlCoCrFeNi high entropy alloys by spark plasma sintering [J]," Materials Review **30**(22), 95–98+103 (2016).
[22] Y. Yu, F. Q. Xie, T. B. Zhang, H. C. Kou, R. Hu, and J. S. Li, "Microstructure control and corrosion properties of AlCoCrFeNiTi0.5 high-entropy alloy [J]," Rare Metal Materials and Engineering **41**(05), 862–866 (2012).
[23] Y. J. Zhou, Y. Zhang, Y. L. Wang *et al.*, "Solid solution alloys of AlCoCrFeNiTix with excellent room-temperature mechanical properties," Applied Physics Letters[J] **90**(18), 1–4 (2007).

[24] J. Zhang, The Microstructure and Performance of High-Entropy Alloys Alx CoCrFeNiTi$_{0.5}$ [D]. Dalian University of Technology, 2013.
[25] Y. Wang, The Study of Microstructures and Mechanical Properties of AlCoCrFeNiTi_x High-entropy Alloys [D]. Taiyuan University of Technology, 2013.
[26] X. Mao, Study on Microstructure and Properties of the as-CAST and Annealing AlCoCrFeNiTi_x High Entropy Alloy [D]. Guangxi University, 2013.
[27] J. Antonio, S. Egea, A. Hernán, G. Rojas, D. J. Celentano, and J. J. Peiró, "Mechanical and metallurgical changes on 308L wires drawn by electropulses[J]," Materials and Design **90**, 1159–1169 (2016).
[28] N. Zhisheng, H. Li, and J. Wang, "Thermal stability of AlCrFeNiTi high entropy alloy [J]," Rare Metal Materials and Engineering **47**(01), 191–196 (2018).
[29] J. Yang, P. Q. La, W. M. Liu, and Q. J. Xue, "Tribological properties of FeAl intermetallics under dry sliding," Wear[J] **257**(1-2), 104–109 (2004).
[30] J. Cheng, F. Li, L. C. Fu, Z. H. Qiao, J. Yang, and W. M. Liu, "Dry-sliding tribological properties of TiAl/Ti 2 AlC composites[J]," Tribology Letters **53**(2), 457–467 (2014).
[31] Y. H. Kang, J. Yang, L. C. Fu, Q. L. Bi, and W. M. Liu, "Mechanical properties and dry-sliding tribological behavior of partially twinned Fe 70 Ni 30 alloy[J]," Wear **274**, 395–400 (2012).
[32] P. Zhang and Y. Wang, "Effects of heat treatment on the nanoscale precipitation behavior of 7055 aluminum alloy under dynamic shock[J]," Vacuum **152**, 150–155 (2018).
[33] P. Zhang and Y. Wang, "Effects of shear strain and annealing on the nano-precipitate phase and crystal orientation of 7055 aluminum alloy during cutting process[J]," Vacuum **15**, 247–253 (2018).